

FIG. 2. Hall mobility as a function of the electric field.

ary condition and thereby obtain different field values for the high-field domain in the same crystal as was done, for example, in Ref. 7. However, the fact that the low-field value of the mobility, μ (230°K) = 620 cm²/V sec, of all crystals used agrees well with the value attributed to phonon scattering and obtained by several

other investigators,¹¹ and the similar trend of $\mu(E)$ at higher fields indicates that the slightly different doping has no significant effect on the Hall mobility for all investigated crystals in the entire measured range.

Therefore, before better results for one and the same CdS crystal are available it seems legitimate to assume the values of μ as given in Fig. 2 to describe the field-dependent mobility $\mu(E)$ for not-too-heavily doped CdS platelets. Up to about 30 kV/cm the mobility seems to remain field-independent; then the mobility decreases approximately in proportion to E^{-1} . This behavior is in agreement with the theory of hot-electron scattering with optical phonons.

We would like to acknowledge the doping of two crystals by P. Voss and are grateful for many discussions with P. Voss and G. Dussel. We appreciate the use of an electromagnet by courtesy of Dr. M. Sharnoff and Dr. R. Ewing.

¹¹ W. W. Piper and R. E. Halsted, in *Proceedings International Conference Semiconductors, Prague, 1960* (Czechoslovak Academy of Sciences, Prague, 1961), p. 1046; K. Kobayashi, H. Fujita, and T. Kawai, *J. Phys. Soc. Japan* **19**, 135 (1964).

X-Ray Determination of the Electron Momentum Density in Diamond, Graphite, and Carbon Black

RICHARD J. WEISS

Materials Research Laboratory, Army Materials and Mechanics Research Center, Watertown, Massachusetts 02172

AND

WALTER C. PHILLIPS

National Aeronautics and Space Administration Electronics Research Center, Cambridge, Massachusetts 02139

(Received 3 July 1968)

The Compton profile has been measured with the x-ray scattering vector along five selected crystallographic directions in diamond, in polycrystalline diamond, in carbon black, and with the x-ray scattering vector along three selected directions in pyrolytic graphite. The electron momentum densities in both diamond and graphite are more extended in momentum space than a superposition of Hartree-Fock $1s^22s2p^3$ free-atom momentum densities, with the diamond momentum density more extended than the graphite. The momentum densities of carbon black and graphite are similar, as expected from an earlier x-ray diffraction investigation of their crystal structures. The small anisotropies found in the diamond momentum density can be qualitatively explained by assuming that some momentum density at high momentum values in momentum space has been transferred from the $\langle 211 \rangle$ directions to the $\langle 100 \rangle$ directions. The small anisotropy measured in graphite is in marked contrast to the large anisotropy found in positron-annihilation measurements. In addition, the momentum density of graphite deduced from positron annihilation is less extended in momentum space than that deduced from the x-ray measurements. As suggested by Berko, these results give insight into the positron wave function and its perturbation of the annihilated electron. In diamond, the momentum densities deduced from positron annihilation and the Compton profile are similar.

INTRODUCTION

SOME exploratory work in determining the ground-state electron momentum density from the x-ray Compton profile has been reported for Li, Be, B, LiF, Na, Mg, and Al.¹ In the experiments reported here on

diamond, graphite, and carbon black, an effort has been made to decrease the statistical uncertainty in order to detect differences between diamond and graphite as well as the anisotropy in each. In previous work at lower resolution Cooper and Leake² did not report any such

¹ Walter C. Phillips and R. J. Weiss, *Phys. Rev.* **171**, 790 (1968).

² Malcolm Cooper and J. A. Leake, *Phil. Mag.* **15**, 1201 (1967).

TABLE I. Experimental $J(z)$ values (z is the electron momentum in atomic units) for carbon black; pyrolytic graphite averaged over the three measured directions; diamond powder; diamond averaged around the $[110]$ axis; diamond $[110]$, $[111]$, $[100]$, $[211]$, and $[221]$; pyrolytic graphite c axis and 90° and 45° to the c axis. The final column gives the Hartree-Fock (HF) $J(z)$ values for the free-atom $1s^2 2s 2p^3$. The experimental values of J beyond $z=1.6$ a.u. are essentially identical for all cases. The absolute uncertainty in the experimental value of J is ± 0.02 (a.u.) $^{-1}$ for all values of z . The relative uncertainty is ± 0.01 (a.u.) $^{-1}$ (1 a.u. = $mc/137$).

z	Carbon black	Graphite ave.	Diamond powder	Diamond ave.	Diamond					Graphite			HF $1s^2 2s 2p^3$
					$[110]$	$[111]$	$[100]$	$[211]$	$[221]$	c axis	90°	45°	
0.00	2.23	2.16	2.08	2.05	2.11	2.05	2.09	2.04	2.02	2.14	2.15	2.18	2.55
0.04	2.20	2.17	2.09	2.05	2.10	2.03	2.11	2.05	2.02	2.15	2.18	2.18	
0.08	2.19	2.17	2.09	2.05	2.08	2.00	2.12	2.06	2.03	2.16	2.18	2.17	
0.12	2.18	2.17	2.06	2.05	2.08	1.99	2.10	2.06	2.05	2.16	2.18	2.16	
0.16	2.18	2.15	2.05	2.04	2.08	2.00	2.07	2.05	2.05	2.14	2.16	2.14	
0.20	2.15	2.12	2.04	2.03	2.05	2.00	2.07	2.04	2.01	2.12	2.12	2.12	2.46
0.24	2.11	2.10	2.03	2.01	2.01	1.98	2.08	2.02	1.97	2.11	2.09	2.09	
0.28	2.08	2.07	2.01	1.99	1.99	1.99	2.08	2.00	1.96	2.08	2.07	2.07	
0.32	2.05	2.05	1.99	1.97	1.97	1.96	2.01	1.98	1.94	2.04	2.04	2.06	
0.36	2.03	2.02	1.96	1.94	1.97	1.92	1.94	1.94	1.93	2.02	2.01	2.05	
0.40	1.99	1.99	1.93	1.91	1.93	1.89	1.91	1.91	1.92	1.99	1.98	2.00	2.18
0.44	1.94	1.94	1.89	1.89	1.87	1.89	1.90	1.89	1.89	1.96	1.95	1.93	
0.48	1.89	1.89	1.85	1.86	1.83	1.86	1.89	1.86	1.85	1.92	1.90	1.89	
0.52	1.84	1.86	1.81	1.82	1.79	1.84	1.84	1.82	1.83	1.87	1.86	1.85	
0.56	1.80	1.81	1.78	1.79	1.74	1.80	1.78	1.79	1.79	1.82	1.81	1.81	
0.60	1.73	1.76	1.74	1.74	1.69	1.77	1.73	1.75	1.74	1.77	1.75	1.75	1.77
0.64	1.67	1.70	1.68	1.70	1.64	1.72	1.68	1.70	1.70	1.72	1.68	1.69	
0.68	1.61	1.64	1.63	1.65	1.60	1.68	1.63	1.65	1.65	1.65	1.63	1.63	
0.72	1.56	1.57	1.58	1.60	1.54	1.62	1.57	1.60	1.61	1.58	1.56	1.58	
0.76	1.50	1.51	1.52	1.54	1.50	1.57	1.51	1.55	1.55	1.53	1.49	1.51	
0.80	1.44	1.44	1.47	1.48	1.44	1.50	1.46	1.48	1.49	1.45	1.43	1.44	1.34
0.84	1.36	1.36	1.42	1.42	1.39	1.45	1.39	1.42	1.43	1.37	1.36	1.36	
0.88	1.30	1.29	1.36	1.37	1.35	1.39	1.33	1.37	1.38	1.29	1.28	1.31	
0.92	1.24	1.23	1.30	1.31	1.30	1.32	1.27	1.30	1.33	1.23	1.23	1.24	
0.96	1.18	1.17	1.25	1.25	1.25	1.25	1.22	1.25	1.28	1.15	1.17	1.17	
1.00	1.10	1.10	1.18	1.19	1.20	1.18	1.16	1.19	1.22	1.09	1.10	1.10	0.99
1.10	0.96	0.95	1.04	1.04	1.06	1.04	1.00	1.03	1.06	0.93	0.96	0.95	
1.20	0.82	0.82	0.88	0.88	0.91	0.88	0.86	0.87	0.89	0.80	0.83	0.82	0.74
1.30	0.70	0.71	0.76	0.76	0.79	0.76	0.74	0.75	0.77	0.70	0.72	0.71	
1.40	0.59	0.61	0.64	0.65	0.66	0.65	0.64	0.64	0.64	0.61	0.61	0.61	0.56
1.50	0.52	0.54	0.55	0.55	0.56	0.55	0.54	0.55	0.55	0.54	0.53	0.54	
1.60	0.46	0.47	0.47	0.47	0.47	0.47	0.47	0.47	0.47	0.47	0.47	0.47	0.45

differences. While the differences between the measured Compton profile for diamond (and graphite) and that calculated for a superposition of Hartree-Fock free-atom momentum densities are large, the measured differences between diamond and graphite and the anisotropies in each are small.

EXPERIMENT

The experimental arrangement was identical to that described previously.¹ A Mo-target spectrographic x-ray tube, a LiF crystal analyzer (400), and a Compton scattering angle $2\theta_c$ of 117° were employed. Measurements on diamond were made on a gem-quality single-crystal octahedron of 6.4 carats and on a coarse mesh powder. The search for anisotropy in graphite was made on pyrolytic graphite with a c -axis rocking curve of $\sim 5^\circ$. The carbon black sample was a pressed specimen of Cabot Vulcan-9 (175 Å particle size).

Measurements on diamond were made in five directions, i.e., with the x-ray scattering vector along the $[110]$, $[100]$, $[111]$, $[211]$, and $[221]$ directions. Three directions were employed in pyrolytic graphite; 10° , 45° , and 90° to the c axis. The c axis itself was avoided since in this orientation Bragg scattering from the continuum overlapped the tail of the Compton line.

However, the measured anisotropy is quite small and the 10° direction is assumed to be sufficiently representative of the c axis. Counting rates at the center of the Compton line were about 1000 x rays/min and data were taken at intervals of ~ 0.018 (a.u.) in momentum space ($0.01^\circ 2\theta$ of the LiF analyzer). Many runs were made in each direction so that at least 50 000 x rays per datum point were accumulated near the peak.

RESULTS

In obtaining the results described below the $K\alpha_1$ Compton component was separated from the measured Compton profile (corrected for sample absorption and with background subtracted) using the Rachinger method,³ and the effects of finite instrumental resolution were removed by a procedure previously described, yielding $J(z)$, i.e., the Compton profile converted to an electron momentum scale z and normalized.¹ In polycrystalline samples such as diamond powder and carbon black the momentum density is an average over all directions in momentum space, and therefore only depends on the magnitude of the electron momentum. This quantity, defined as the radial momentum density

³ W. A. Rachinger, J. Sci. Instr. 25, 254 (1948).

TABLE II. A continuation of Table I for the higher momentum values.

z	$J(z)$ Expt.	HF $1s^22s2p^3$
1.8	0.37	0.36
2.0	0.31	0.31
2.2	0.27	0.27
2.4	0.24	0.24
2.6	0.23	
2.8	0.22	
3.0	0.20	0.16
3.5	0.17	0.13
4.0	0.13	0.09
4.5	0.10	
5.0	0.08	0.06
5.5	0.05	
6.0	0.04	0.03
6.5	0.02	
7.0	0.01	0.02

$4\pi|\chi|^2$ (i.e., radial in momentum space not real space), can be obtained from the slope of the $J(z)$ curve;

$$4\pi|\chi|^2 = \left| \frac{2}{z} \frac{dJ}{dz} \right|. \quad (1)$$

The experimental results for $J(z)$ are presented in Tables I and II. Figure 1 shows $J(z)$ folded about $z=0$ for the $[111]$ and $[110]$ directions in diamond, for carbon black, and for a superposition of Hartree-Fock free-atom momentum densities $1s^22s2p^3$ and $1s^2$ (core). (The sp^3 valence-electron configuration was selected for comparison rather than the ground-state s^2p^2 since it gives better agreement with our experiment and is commonly employed in considerations of carbon bonding.) There are several features to be noted.

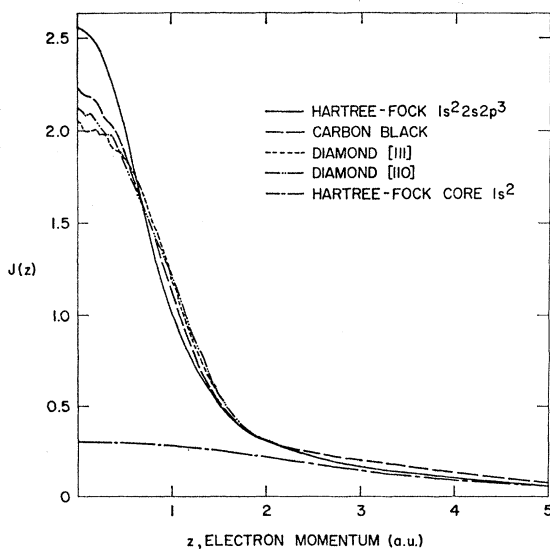


FIG. 1. Compton line shapes for carbon. Experimental $J(z)$ curves folded about $z=0$ (z is the electron momentum in atomic units) for the $[111]$ and $[110]$ directions in diamond and for carbon black; calculated $J(z)$ curves for a superposition of Hartree-Fock free atom momentum densities ($1s^22s2p^3$) and for the $1s^2$ alone.

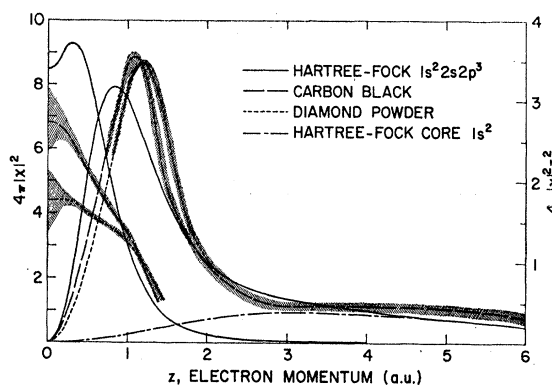


FIG. 2. Spherically averaged momentum densities per atom $4\pi|\chi|^2$ for diamond powder, carbon black, and a Hartree-Fock $1s^22s2p^3$ (left-hand curves). The curves to the right are the radial momentum density $J(z)=4\pi|\chi|^2 z^2$, for which the calculated Hartree-Fock core $1s^2$ is also plotted. Because of the large uncertainty in determining $|\chi|^2$ near the origin, the data have been extrapolated to $z=0$ (thin lines). The shading indicates the estimated experimental uncertainty.

(1) The measured $J(z)$ curves for diamond and carbon black are significantly broader than those calculated for a superposition of free-atom momentum densities.

(2) The anisotropies in diamond are small compared to the large change between the free atom and the crystal.

(3) There is noticeable "structure" in the measured $J(z)$ curves at low values of momentum. As expected, this structure was found in symmetric positions about the center of the Compton line ($z=0$).

(4) There is an appreciable "tail" in the valence electron contribution for z values (electron momentum) from ~ 3 to ~ 5 (a.u.).

ANALYSIS OF RESULTS

This analysis is aimed primarily at providing conceptual pictures of the momentum densities.

It is fairly straightforward to determine the radial momentum density from the polycrystalline measurements since these average over the angular variable.⁴ In Fig. 2 are given the radial momentum densities $4\pi|\chi|^2$ and the momentum distributions $4\pi|\chi|^2 z^2$ for diamond powder, carbon black, the Hartree-Fock⁴ free-atom $1s^22s2p^3$, and the Hartree-Fock free-atom core $1s^2$. In spite of the many calculations of crystalline diamond wave functions, no calculation of the momentum density has been published.⁵

In order to analyze the small anisotropies in the momentum density we proceeded as follows: Diamond measurements were made with the scattering vector along five selected directions normal to the $[110]$ axis, i.e., $[1\bar{1}0]$, $[001]$, $[1\bar{1}2]$, $[2\bar{2}1]$, and $[1\bar{1}1]$. The $J(z)$ curves for these directions were averaged by appro-

⁴ R. J. Weiss, A. Harvey, and Walter C. Phillips, *Phil. Mag.* **17**, 241 (1968).

⁵ I. Goroff and L. Kleinman, *Phys. Rev.* **164**, 1100 (1968).

priately weighting the separate results so as to approximate the curve that one would obtain if the diamond were continuously rotated around the $[110]$ axis during the measurement. The differences between each direction and this average, $\Delta J(z)$, are plotted in Fig. 3(a). Each point on a curve represents the difference from the average of a $[110]$ planar projection of the momentum density at a distance z from the origin in momentum space. (Since all curves are normalized, positive and negative areas are equal.) After some trial and error it was found that the gross features of these curves could be reproduced by transferring some momentum density in the vicinity of 1.3–2.3 (a.u.) along the $\langle 211 \rangle$ directions to similar regions along the $\langle 100 \rangle$ directions. This is qualitatively shown in Fig. 3(a), where the holes along the $\langle 211 \rangle$ directions are unshaded and the positive regions along $\langle 100 \rangle$ are shaded. Note that the nearest-neighbor direction is along the body diagonal $[111]$, and that the $\langle 211 \rangle$ and $\langle 100 \rangle$ directions each form a simple trigonal arrangement around the $[111]$. If in fact the anisotropy is confined to specific regions of momentum density, it is obvious that the momentum density can not be written as a simple product of functions depending solely on angular and radial variables in momentum space.

In a similar way to diamond the anisotropies in graphite are shown in Fig. 3(b) as differences between the measured $J(z)$ curve in each of the three directions and the averaged curve for the three directions. This averaged curve corresponds essentially to a projection

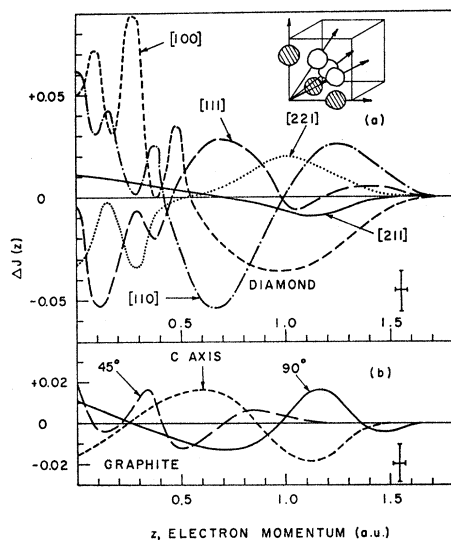


FIG. 3. (a) Experimental difference curves $\Delta J(z)$ between the $J(z)$ for the five directions in diamond ($[110]$, $[111]$, $[100]$, $[211]$, and $[221]$) and the $J(z)$ curve averaged around the $[110]$ axis. (b) Experimental difference curves $\Delta J(z)$ between the $J(z)$ for the three directions in pyrolytic graphite (c axis, 45° and 90° to the c axis) and the $J(z)$ curve averaged over these directions. The inset shows an approximate distribution of negative (unshaded) and positive (shaded) momentum density which yields the gross features of the $\Delta J(z)$ curves for diamond. The error bars are in the lower right-hand corners.

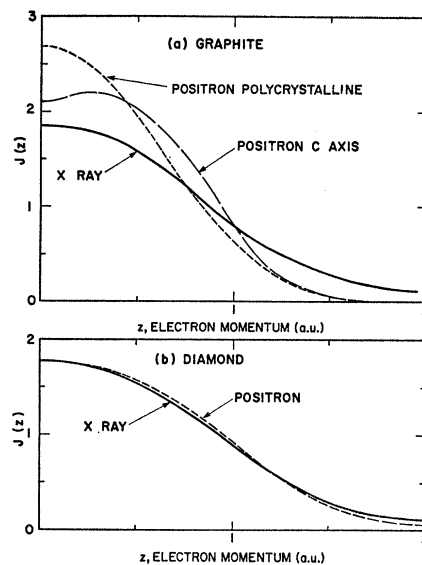


FIG. 4. X-ray Compton profiles and positron line shapes for the valence electrons (i.e., with the $1s^2$ core subtracted in the x-ray case) in (a) graphite and (b) diamond powder. The positron measurements on graphite made along the c axis and on polycrystalline graphite reveal a large anisotropy, whereas the anisotropy in the Compton profiles from pyrolytic graphite is too small to show on this scale.

of the momentum density onto a plane normal to the c axis. The nature of the random stacking of planes in pyrolytic graphite is such that each measurement also averages around the c axis. The anisotropy is considerably smaller than in diamond and no attempt was made to devise a momentum density that would reproduce the curves in Fig. 3(b).

DISCUSSION

Two other sets of measurements provide information pertinent to these Compton line-shape measurements: (a) the angular correlation of the positron-annihilation γ rays from diamond and graphite,^{6–8} and (b) the x-ray structure factor measurements on diamond⁹ (there are no reliable measurements for graphite or carbon black). In Fig. 4 are shown the positron and Compton x-ray measurements for diamond and graphite. While the diamond results reveal only a small difference between the two types of measurements, in graphite the differences are extremely large. In addition, the anisotropy in the positron measurement is quite striking for graphite. It seems likely, as suggested by Berko, that the differences between the x-ray results and the positron results arise from two causes: (a) the Coulomb

⁶ G. Lang and S. de Benedetti, Phys. Rev. **108**, 911 (1957).

⁷ S. Berko, R. E. Kelley, and J. S. Plaskett, Phys. Rev. **106**, 824 (1957).

⁸ S. Berko and J. C. Erskine (private communication) have recently measured positron-annihilation profiles on the same diamond and graphite samples used in our x-ray experiments and found agreement with the previously reported measurements (Refs. 6 and 7).

⁹ S. Göttlicher and E. Wölfel, Z. Elekt. **63**, 891 (1959).

perturbation of the annihilated electron by the positron and (b) the details of the positron wave function. It is not obvious how one separates (a) and (b).

There are two Bragg reflections in diamond with significant valence-electron contributions, (111) and (222), the latter reflection due solely to the anisotropic part of the charge density. There have been many calculations of the charge density of diamond which yield reasonable agreement with the (111) and (222) structure factors,⁵ but as stated above no calculations of momentum density are available. An empirical approach to the problem of analyzing the charge-density anisotropy has been given by Weiss¹⁰ and by Dawson.¹¹ A wave function with one or more adjustable parameters is expanded in terms of functions with the appropriate crystal symmetry. The leading term in such an expansion for diamond is

$$\psi = A(R_1 + (\alpha xyz/r^3)R_2), \quad (2)$$

where A is the normalization factor, R_1 and R_2 are radial wave functions, and α is an adjustable parameter. This leads to a charge density pointing toward the four nearest-neighbor ($[111]$, $[\bar{1}\bar{1}\bar{1}]$, $[\bar{1}\bar{1}1]$, and $[\bar{1}1\bar{1}]$) directions and yields a scattering factor

$$f = \langle j_0(sr) \rangle - \frac{2i\alpha hkl}{(h^2 + k^2 + l^2)^{3/2}} \langle j_3(sr) \rangle + \text{higher terms}, \quad (3)$$

where

$$\langle j_0(sr) \rangle = \int R_1^2 j_0(sr) r^2 dr,$$

$$\langle j_3(sr) \rangle = \int R_1 R_2 j_3(sr) r^2 dr,$$

$j_0(sr)$ and $j_3(sr)$ being spherical Bessel functions and $s = (4\pi \sin\theta)/\lambda$. Equation (2) yields a momentum function for any direction uvw

$$\chi = \frac{4\pi A}{(2\pi)^{3/2}} \left\{ \hat{j}_0(pr) - \frac{i\alpha uvw}{(u^2 + v^2 + w^2)^{3/2}} \hat{j}_3(pr) \right\}, \quad (4)$$

where

$$\hat{j}_0(pr) = \int R_1 j_0(pr) r^2 dr,$$

$$\hat{j}_3(pr) = \int R_2 j_3(pr) r^2 dr.$$

The momentum density $|\chi|^2$ points toward the body diagonals in the crystal. (The charge density is not

centrosymmetric but the momentum density is.) The Compton profile calculated from Eq. (4) is, for any direction uvw ,

$$J(z) = 2A^2 \int_{|z|}^{\infty} (\hat{j}_0(pr))^2 p dp + \frac{A^2 \alpha^2}{32} \int_{|z|}^{\infty} (\hat{j}_3(pr))^2 \left\{ \frac{1 + (w/u)^4}{[1 + (w^2/2u^2)]^3} + \frac{z^2}{p^2} \left[8 - \frac{15(1 - (w/u)^2 + (w/u)^4)}{[1 + (w^2/2u^2)]^3} + \frac{z^4}{p^4} \left[\frac{35 - 70(w/u)^2 + 35(w/u)^4}{[1 + (w^2/2u^2)]^3} - 16 \right] + \frac{z^6}{p^6} \left[8 - \frac{21 - 71(w/u)^2 + 21(w/u)^4}{[1 + (w^2/2u^2)]^3} \right] \right\} p dp. \quad (5)$$

By assuming $R_1 = R_2$, where R_1 is the radial part of a Hartree-Fock $2p$ wave function for carbon, and $\alpha \cong 1$, one can obtain reasonable agreement with the measured (111) and (222) structure factors.⁵ However, the Compton line shapes so calculated evidence negligible anisotropy (less than $\frac{1}{10}$ the measured anisotropy) and are in fact not noticeably different from the free-atom calculations (Fig. 1). Furthermore, the momentum density peaks in the $[111]$ direction, in contrast to the observations (Fig. 3). The complexity of the anisotropy of momentum density in momentum space appears to make such an empirical approach impracticable.

The similarity in the line shapes for graphite and carbon black is consistent with the observations of Biscoe and Warren¹² that carbon black is essentially a very finely dispersed graphite structure, i.e., small graphite regions with very little a -axis correlation. Thus the electron distribution, which is governed by the near neighbors, would be expected to be essentially identical in both.

ACKNOWLEDGMENTS

We wish to thank George Kaplan of Lazare Kaplan and Sons, New York, for providing the diamond crystal, Mrs. Anna Hansen for programming the many calculations required for the various figures, and Professor S. Berko and Professor J. C. Erskine for allowing us to quote their unpublished results on diamond and graphite. We profited from helpful discussions with Dr. Ralph Harrison.

¹⁰ R. J. Weiss, Phys. Letters **12**, 293 (1964).

¹¹ B. Dawson, Proc. Roy. Soc. (London) **A298**, 264 (1967).

¹² J. Biscoe and B. E. Warren, J. Appl. Phys. **13**, 364 (1942).